Sensors and Materials, Vol. 34, No. 4 (2022) 1601–1615
MYU Tokyo

S & M 2913

Multichannel Bandpass Filters for Reconstructed High-resolution Spectral Imaging in Near-infrared Fundus Camera

Honghao Tang,[1] Hironari Takehara,[1*] Ze Wang,[1] Noriaki Kishida,[1]
Makito Haruta,[1] Hiroyuki Tashiro,[1,2] Kiyotaka Sasagawa,[1] and Jun Ohta[1]

[1]Division of Materials Science, Graduate School of Science and Technology,
Nara Institute of Science and Technology, 8916-5 Takayama, Ikoma, Nara 630-0192, Japan
[2]Division of Medical Technology, Department of Health Sciences, Faculty of Medical Sciences,
Kyushu University, 3-1-1 Maidashi, Higashi-Ku, Fukuoka 812-8582, Japan

(Received November 30, 2021; accepted March 8, 2022)

Keywords: optical design, multichannel imaging, interference filter, spectral reconstruction, fundus camera, near-infrared

Diagnosis by ocular fundus imaging plays a key role in the monitoring, detection, and diagnosis of several diseases including eye-related, hypertensive, and cardiovascular diseases as well as the detection of brain microvascular and neuronal pathology. The spectral detection of the fundus in the near-infrared (NIR) region can be used to analyze the composition and content of the fundus substance. The aim of this study was to develop a multichannel bandpass filter, which can be assembled on a CMOS image sensor installed in a fundus camera, to realize spectral imaging. We designed the filter in the NIR region according to interference filter theory and fabricated it by sputtering, lithography, and etching. The images acquired by the image sensor with the fabricated bandpass filter confirmed that the pixel values were comparable to the values calculated from spectrometer measurements. In an experimental validation, the number of measurement wavelengths was increased by applying the incident angle dependence of the interference filter. Each fabricated filter had a relatively wide transmittance band for spectral detection, broadening the spectrum curve. Moreover, a high-resolution spectrum was reconstructed using the developed algorithm. The spectrum reconstructed by the proposed filter had a 15% average relative error over the entire wavelength range of interest.

1. Introduction

Ocular fundus imaging plays a key role in the monitoring of human health. The retina may be the only part of the body where blood vessels can be directly observed, making it possible to directly observe the biochemical activities in the body.(1) By examining fundus images, eye-related diseases can be diagnosed, and the detection, diagnosis, and management of hypertensive and cardiovascular diseases are possible.(2,3) Anatomically and developmentally, the retina is an extension of the brain.(4) Therefore, the diagnosis of the fundus can be used as an alternative means of detecting brain microvascular and neuronal pathology.(5,6)

*Corresponding author: e-mail: t-hironari@ms.naist.jp
https://doi.org/10.18494/SAM3759

ISSN 0914-4935
https://myukk.org/

Color fundus cameras, scanning laser ophthalmoscopy, and, more recently, optical coherence tomography (OCT) have been used to diagnose and screen for ocular-related diseases. Different devices have different advantages and disadvantages. For instance, OCT is suitable for determining the thickness of the retina but not blood oximetry. In general, fundus cameras can be miniaturized for portability, and smartphone-based fundus cameras are already in use.[7–9] However, most fundus cameras use visible light for illumination; therefore, obtaining continuous or long-term fundus video images can be very difficult. In addition, momentary intense light may cause dizziness and eye discomfort.[10]

In our previous study, we proposed a selfie fundus camera that can work in the near-infrared (NIR) region and obtain a colorized image.[10,11] Because the eye is not sensitive to NIR light, the proposed fundus camera can avoid eye stimulation. Moreover, to observe the blood vessels, the optic disc, and other tissues, we also proposed a noninvasive method for retinal scattering detection using a patterned interference filter in our NIR fundus camera.[12] By using thin-film interference filters, we added the function of spectral detection to our NIR fundus camera.

Changes in light scattering and/or absorption properties in retinal tissues are often accompanied by retinal pathological changes and retinal-related diseases.[13] Studies indicate the presence of many biomarkers in retinal vessels and their surrounding tissues, such as oxygen saturation (sO_2), macular pigment absorption, and the cell protein oxidative state. These substances have different spectra because of optical scattering and absorption.[14–19] From spectral imaging, researchers can study the metabolism and chemical structure in human tissue, including changes that occur in diabetes and diabetic retinopathy.[20] Spectral images enable qualitative and quantitative analyses of different components in the retina.[13]

Hyperspectral imaging can capture narrow spectral bands over a continuous spectral range. Hyperspectral retinal imaging can increase the quality of diagnosis. However, the clinical application of hyperspectral retinal imaging is limited by the scanning time and complexity of the imaging system. Commercially available hyperspectral systems collect information by linearly scanning each band and its corresponding spectrum.[18,21] The entire detection process lasts from a few seconds to a few minutes, which is not very suitable for fast-moving eyes.[14,22] Moreover, existing systems are usually bulky because the beam splitters they use are prisms,[22] multiple apertures, or gratings.[16] This makes it difficult to install or perform self-portrait operations using miniaturized fundus cameras. Although there are also miniaturized snapshot hyperspectral fundus cameras, their working wavelength range is based on visible light.[23,24] At present, a selfie NIR fundus camera with spectral analysis remains to be developed.

In this study, we designed and fabricated a multichannel bandpass filter, which can be assembled on the CMOS image sensor of our NIR fundus camera. We then verified the feasibility of using this filter to detect the spectrum. Subsequently, we present two methods for improving the spectral resolution.

2. Design of Multichannel Bandpass Interference Filter

Commonly available spectrometers use large gratings as spectroscopic devices. Our goal was to design a spectroscopic device that can be installed in a selfie fundus camera, which required a technology for miniaturizing spectroscopic devices.

Interference filters can reflect one or more spectral bands and transmit others while maintaining an absorption coefficient close to zero for all wavelengths of interest. Depending on the type of design, the interference filter can be a bandpass, notch, or edge filter. The Fabry–Perot filter is a bandpass filter that is usually composed of a transparent layer (cavity) with two mirrors on each side.[25] The basic structure of the optical filter consists of a stack of thin films with alternating high and low refractive indices and an optical thickness of a quarter of the target wavelength. When the thickness of the middle layer is half the wavelength, the light phase is inverted and the reflections interfere, transmitting light around the reference wavelength. On the basis of this feature, we were able to control the wavelength of the transmitted light by adjusting the thickness of each layer.

We designed a five-channel bandpass filter based on the theory of interference filters. Figure 1 shows a schematic cross section of the five-channel filter. *H* and *L* represent the quarter-wavelength thicknesses of the high- and low-refractivity materials, respectively. In this study, TiO_2 and SiO_2 were used as high- and low-refractivity materials, respectively, with a total of 13 layers in the five-channel bandpass filter. By modulating the middle-layer thickness, we obtained a five-channel bandpass filter with each channel filtering different transmission wavelength ranges. We designed the NIR bandpass filter channels by simulation using a Mathematica (Wolfram Research, Inc.) program that we developed. The simulated transmittances of the filters are shown in Fig. 2.

3. Experimental Setup and Spectral Reflectance of Imaging Target

Validation experiments were conducted to verify that the constructed bandpass filters and camera, including the CMOS image sensor, correctly measured known spectra. This experiment was conducted by externally using a fabricated filter prior to the construction of the filter array described in Sect. 2. Figure 3 shows the schematic and photograph of the validation system. We used four LEDs as the NIR light source, whose center wavelengths were 780, 810, 850, and 880 nm. The LEDs with adjusted intensities illuminated a diffuse white plate (Spectralon) using the fundus illumination system. The two reflection spectra were measured using a spectrometer

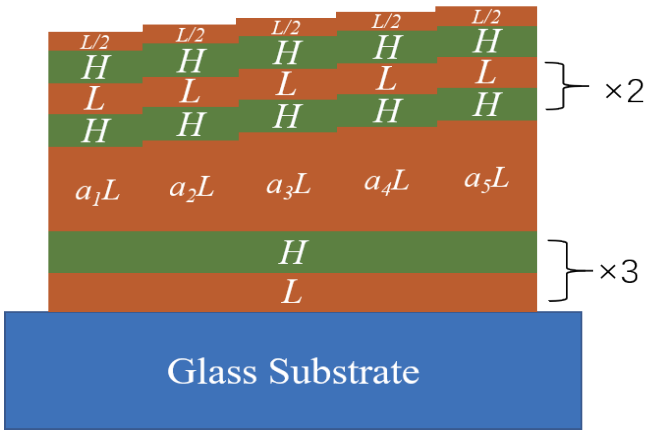

Fig. 1. (Color online) Schematic cross section of the five-channel bandpass filter.

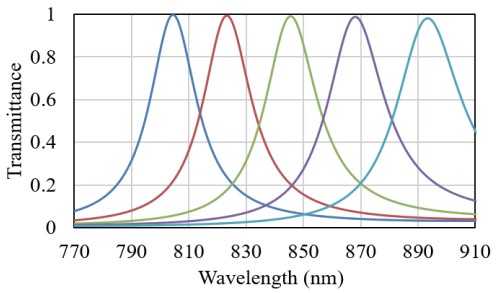

Fig. 2. (Color online) Simulated transmittance spectra of the five-channel bandpass filter.

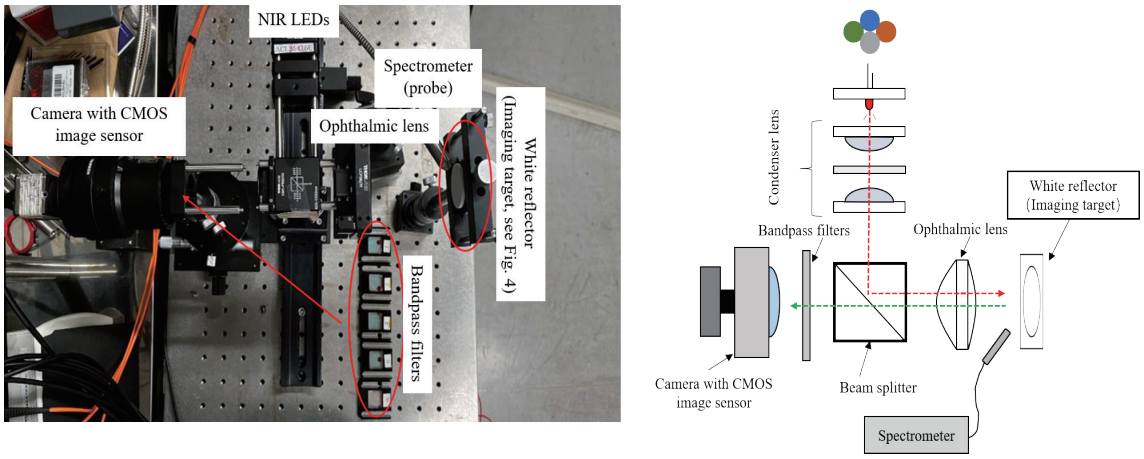

Fig. 3. (Color online) Photograph and schematic of the validation system using a set of five-channel bandpass filters.

(MCPD-3700, Otsuka Electronics Co., Ltd.). We used a camera (DCC3240N, Thorlabs) with a CMOS image sensor to capture multiple images through different bandpass filters. Figure 4(a) shows the reflection image with all LEDs turned on and Fig. 4(b) shows the dark reference image with all LEDs turned off. The pixel values of the reflections were corrected by subtracting the dark level. The pixel values inside the rectangle in Fig. 4 were averaged to obtain the measurement values.

4. Results and Discussion

4.1 Multispectral imaging of uniform reflection targets with known spectra

As described in Sect. 3, we used the verification system to generate two target reflection spectra. Figure 5 shows the original data measured using the spectrometer. The currents set for the 780, 810, 850, and 880 nm LEDs for Reflection 1 were 200, 400, 300, and 500 mA, and those set for Reflection 2 were 300, 200, 400, and 500 mA, respectively. Figures 6(a) and 6(b) respectively show the measured and calculated intensities of each reflection. The intensities were calculated by integrating the original reflection spectra measured using the spectrometer,

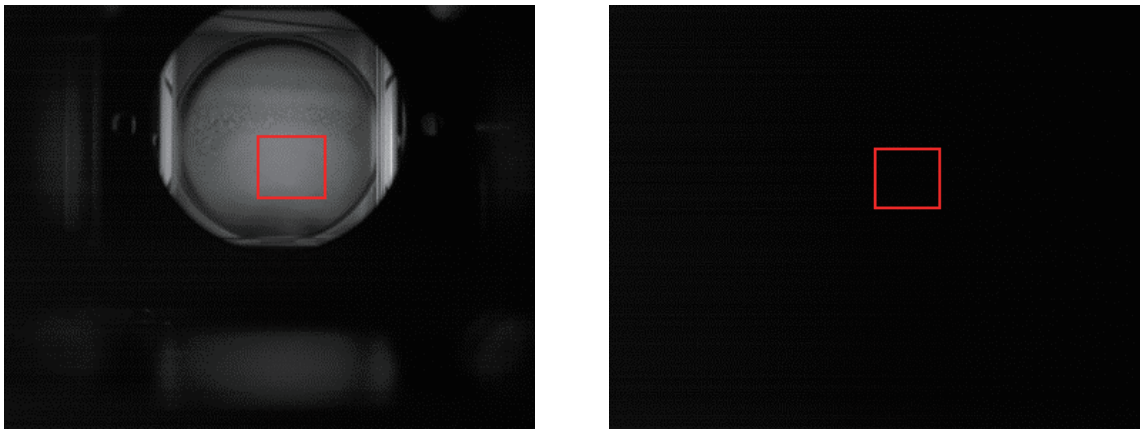

(a) (b)

Fig. 4. (Color online) (a) Image of Reflection 3 with LEDs turned on; (b) dark background (all LEDs turned off). Rectangles represent the region where data was collected.

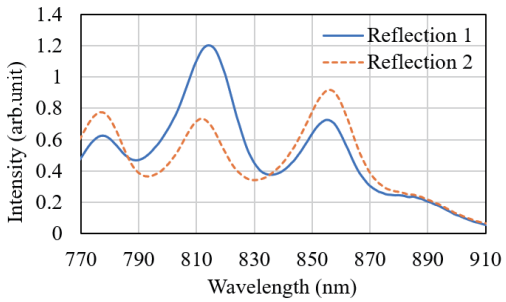

Fig. 5. (Color online) Reflectance spectra of a white diffuser irradiated with a mixture of LED illumination of four wavelengths. Two types of emulated spectra were formed to validate our system.

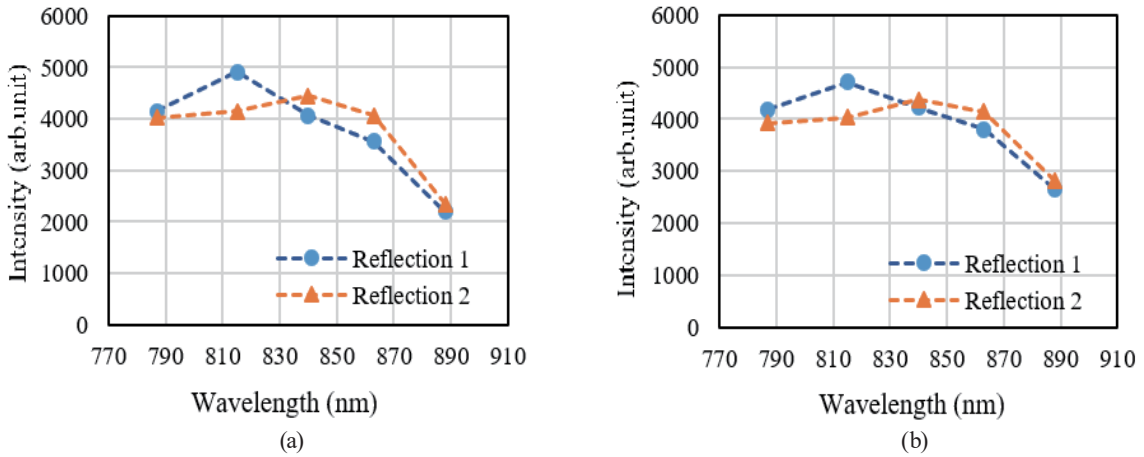

Fig. 6. (Color online) (a) Measured intensities of the two emulated reflections using fabricated filters and CMOS image sensor camera. (b) Calculated intensities of the two emulated reflections by integration of the parameters shown in Fig. 7.

the sensor sensitivity, and the transmittance of each channel, as shown in Figs. 7(a)–7(c), respectively.

By comparing the channel intensity in Figs. 6(a) and 6(b) and the known spectra in Fig. 5, we confirmed that the fabricated filter and image sensor system could detect the spectral signals properly under the experimental conditions.

However, in actual fundus imaging, the imaging conditions are not ideal, as described above. Thus, the correction of non-uniform illumination and noise reduction are issues. We believe that these issues will be overcome mainly by image processing technology.[26]

4.2 Response to changes in spectral intensity

We also examined whether the sensitivity of each image sensor channel varies proportionally with the illumination intensity for complex spectral reflections. The light intensity from the LEDs for Reflection 4 in each band was set exactly halfway between those of Reflections 3 and 5. The setting values for the three reflections are listed in Table 1. Note that we have confirmed that the output intensities of the LEDs change proportionally with the LED current.

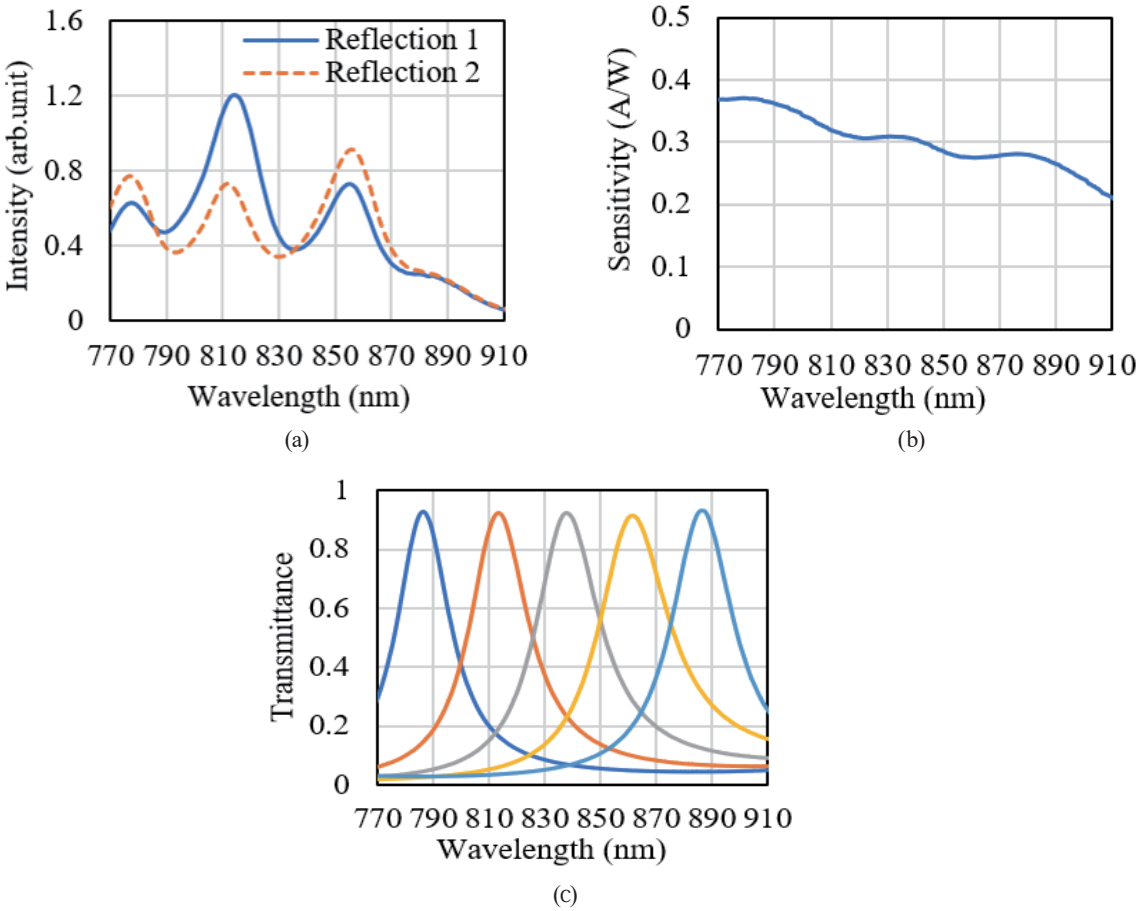

Fig. 7. (Color online) (a) Spectra measured using spectrometer (i_λ), (b) sensitivity of CMOS image sensor (s_λ), and (c) transmittance of each bandpass filter (t_λ). The calculated channel intensity is $\int(i_\lambda \cdot s_\lambda \cdot t_\lambda)d\lambda$.

Table 1
LED currents set to generate emulated reflections with three intensity ratios.

Emulated reflections	LED setting currents (mA)			
	LED_{780}	LED_{810}	LED_{850}	LED_{880}
Reflection 3	200	30	30	350
Reflection 4	115	40	65	425
Reflection 5	30	50	100	500

Figure 8(a) shows the reflection spectra of the five-channel imaging targets of Reflections 3–5 measured using the spectrometer. Figure 8(b) shows the measured data sampled using our system. By comparing the intensity of each channel, it can be seen that the values of Reflection 4 are precisely midway between those of Reflections 3 and 5, indicating that the filter can measure the changes in spectral intensity. In this experiment, gamma correction was not applied. Therefore, we can obtain sensor output values that are proportional to the input intensities.

4.3 Doubling the number of sampling channels

The addition of channels to a fabricated multichannel filter adds complexity to the fabrication process. To determine whether the number of sampling channels used in this experiment was sufficient while limiting the complexity of the fabrication process, we increased the number of channels by using the incidence angle dependence of the interference filter.

Using Eqs. (1)–(3), which describe the reflectivity and transmittance of multilayer thin-film interference filters,[26] the wavelength of the transmitted light can be controlled by changing the incident angle δ_0 while keeping the other parameters unchanged.

$$\begin{bmatrix} B \\ C \end{bmatrix} = \left\{ \prod_{r=1}^{q} \begin{bmatrix} \cos\delta_r & \left(i\sin\delta_r\right)/\eta_r \\ i\eta_r \sin\delta_r & \cos\delta_r \end{bmatrix} \right\} \begin{bmatrix} 1 \\ \eta_m \end{bmatrix} \tag{1}$$

$$Reflectivity = \left(\frac{\eta_0 B - C}{\eta_0 B + C} \right) \left(\frac{\eta_0 B - C}{\eta_0 B + C} \right)^* \tag{2}$$

$$Transmittance = \frac{4\eta_0 Re\left(\eta_m\right)}{\left(\eta_0 B + C\right)\left(\eta_0 B + C\right)^*} \tag{3}$$

Here, η and δ are the admittance and phase thickness, respectively, and the suffixes 0, m, and r denote the incident, substrate, and rth layers, respectively.

Figure 9(a) shows the measured transmittance obtained after tilting the incident angle by 0 and 15°, and Fig. 9(b) shows the ten bandpass intensities measured by the camera at the same two angles. The results indicate that it is possible to increase the resolution by adjusting the incident angle between the filter and the CMOS image sensor.

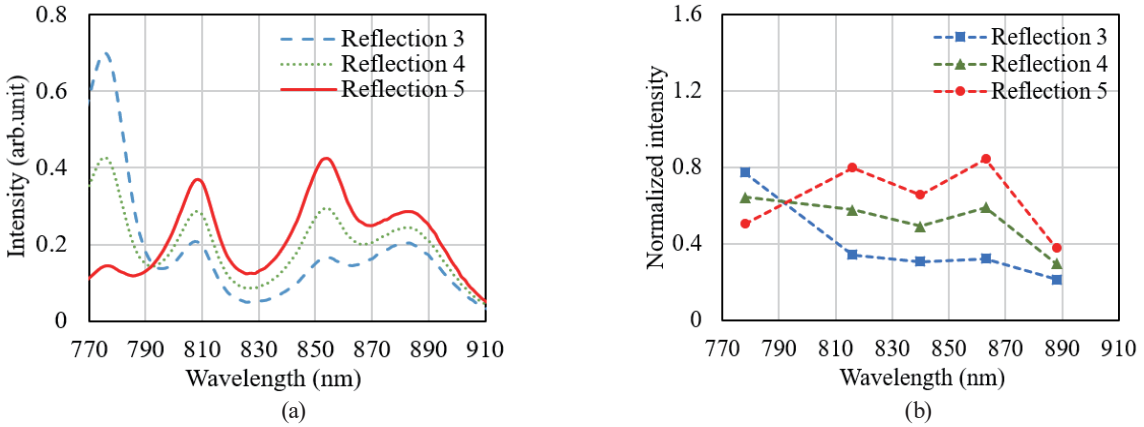

Fig. 8. (Color online) (a) Three target reflection spectra with known changes measured using spectrometer and (b) measured intensities of the three emulated reflections using fabricated filters.

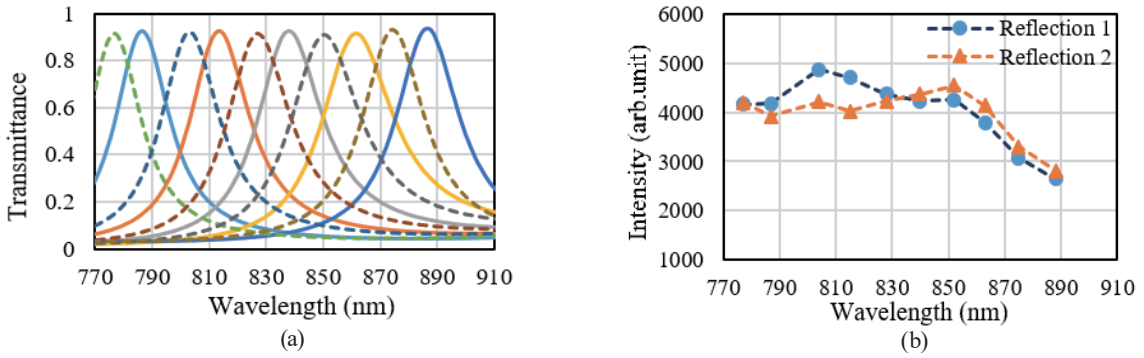

Fig. 9. (Color online) (a) Transmittance of the five-channel bandpass filter at 0 and 15°, and (b) intensity under each channel after increasing the incident angle to 15°. Markers indicate the peak wavelength of each channel.

4.4 High-resolution spectrum reconstruction from measured data

The spectral information obtained by the image sensors is essentially data with a very low resolution. These values can be considered as the convolution of the high-resolution spectral data similar to that shown in Fig. 7, as we have already verified. Therefore, we attempted to reconstruct the information obtained by the image sensor by deconvolution. The deconvolution was executed by estimating the spectrum curve and fitting it to the measured data using the least-squares method. The abbreviations of the symbols are shown in Table 2.

The intensity of each bandpass channel can be expressed as $\hat{I}_{channel} = \int (i_\lambda \cdot s_\lambda \cdot t_\lambda) d\lambda$, where $I_{channel}$, s_λ, and t_λ are known and i_λ is the unknown parameter of interest. Hence, the minimum value of $(\hat{I}_{channel1} - I_{channel1})^2 + \ldots + (\hat{I}_{channel10} - I_{channel10})^2$ yields the target value closest to the actual spectrum value.

The spectral reconstruction algorithm we programmed is a recursive algorithm that uses the least-squares theory. Figures 10(a)–10(c) show the fitting results (dots and squares) along with

Table 2
Abbreviations of symbols.

i_λ	Actual intensity of reflection at specific wavelength λ (search target, unknown)
s_λ	Sensitivity of CMOS image sensor at specific wavelength λ (known)
t_λ	Transmittance of filter at specific wavelength λ (known)
$\hat{I}_{channel,n}$	Intensity of channel n calculated from assumed i_λ (calculated)
$I_{channel,n}$	Measured intensity of channel n (known)

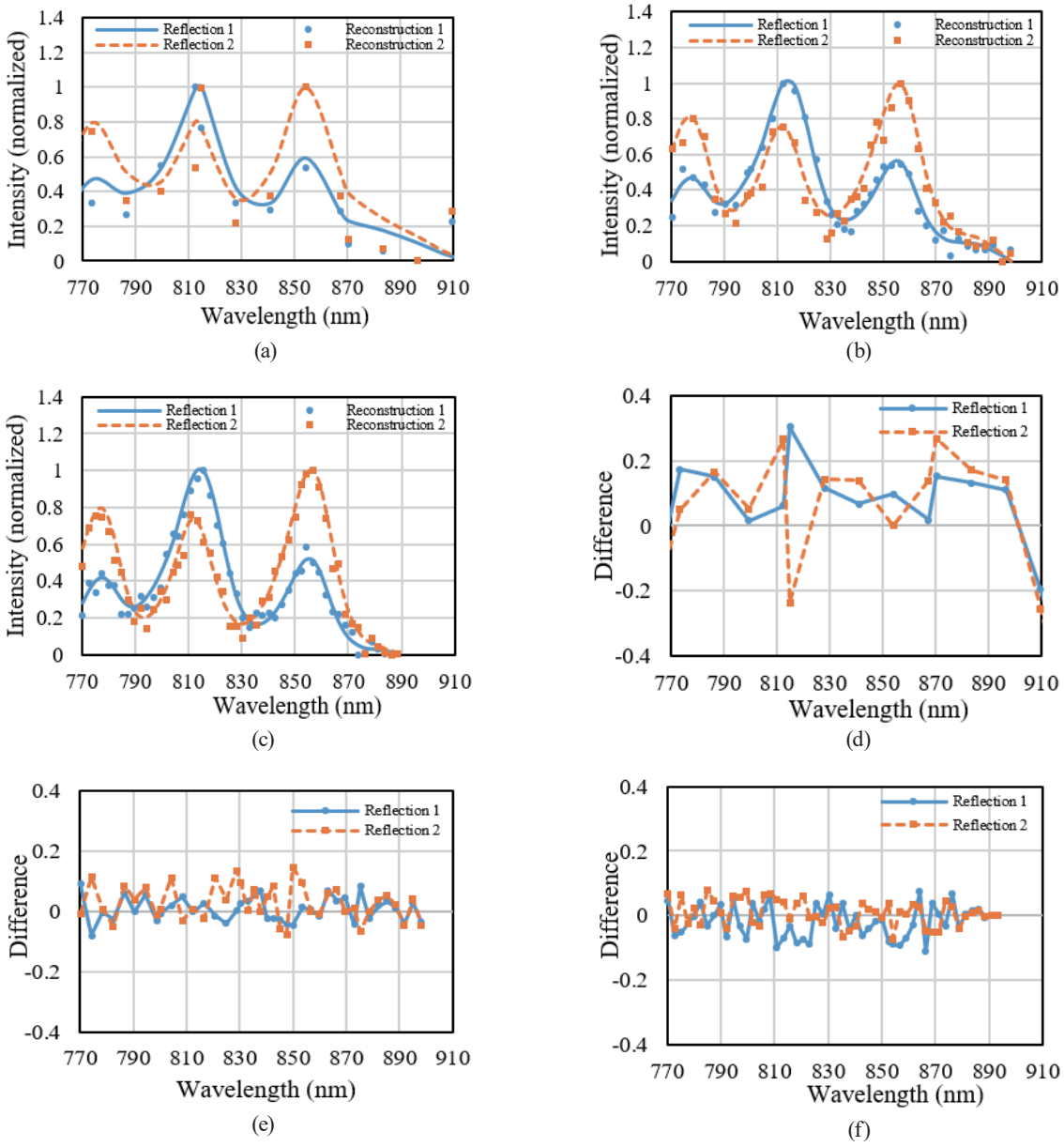

Fig. 10. (Color online) (a) Target reflection and reconstructed data from three channels, (b) reconstructed data from five channels, (c) reconstructed data from ten channels (sampling at incident angles of 0 and 15°), and (d)–(f) difference between reconstructed and original values for three, five, and ten channels applied, respectively.

the original spectra measured using the spectrometer for Reflections 1 and 2 (solid and dashed lines, respectively). The corresponding differences between the reconstructed and original values are shown in Figs. 10(d)–10(f).

It can be seen from the results that with three channels (Channels 1, 3, and 5), the maximum difference is approximately 30%. When five-channel filters were used, the maximum difference decreased to 15%. The maximum difference was further reduced to 10% when the data from ten channels were used. In actual use, the reflectance spectrum of the fundus material will be flatter than our simulated reflection. Therefore, the five-channel spectral data were sufficient for the reconstruction of the spectrum.

Our prototype NIR color fundus camera in the previous work had fixed acquisition wavelengths.[10] Once pixel-by-pixel spectral information is available, images with arbitrary wavelengths can be generated. In other words, it will be possible to select images with the most appropriate wavelength for the corresponding disease or information.

5. Fabrication of Multichannel Bandpass Filter Array with CMOS Image Sensor

Although we used single passband filters fabricated on a single glass substrate in the experiments in Sects. 3 and 4, we also assembled a multichannel bandpass filter for our fundus camera system, as shown in Fig. 11. The filter was constructed on a glass substrate (BDA, Nippon Electric Glass Co., Ltd.). We controlled the thicknesses during sputtering and etching by managing the processing time, which was calculated using preliminarily evaluated sputtering and etching rates. Thus, we used sputtering (CFS-4ES-II, Shibaura), photolithography (MA-10, Mikasa), and etching (RIE-10NIT, Samco) to complete the production of the five-channel bandpass array.

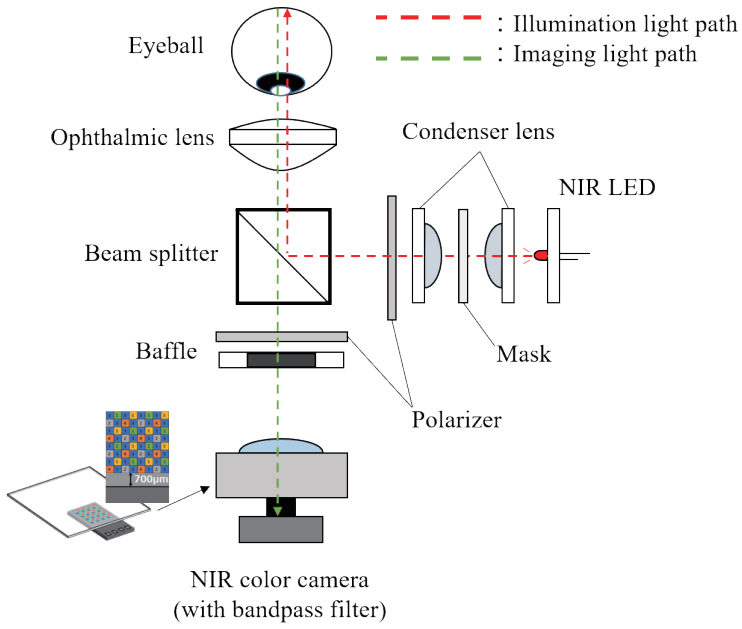

Fig. 11. (Color online) Fundus camera system with a multichannel bandpass filter.

Figure 12 shows a photograph of a mosaic multilayer interference bandpass filter fabricated on a glass substrate. The side length of the filter was 2 mm and the size of each channel was 52.5 μm. We combined this filter array with a CMOS image sensor designed in our laboratory. The CMOS image sensor we used was 256 × 256 pixels with a pixel length of 7.5 μm. In single-shot photography, each image sensor pixel can only obtain information from a single transmission band. However, our fundus camera does not dazzle patients and can capture long videos. The human eye always moves even when we want to fix our eyes (fixational eye movement).[27] Therefore, high-resolution multiband images can be reconstructed by detecting the motion and acquiring all the transmission band information for each fundus position.

Figure 13 shows the appearance of the alignment device and a schematic of the filter adhesion. The alignment device comprises two parts: a glass substrate fixing seat and an image sensor fixing seat. The alignment device was installed on the movable stage (*XY* axis) of the

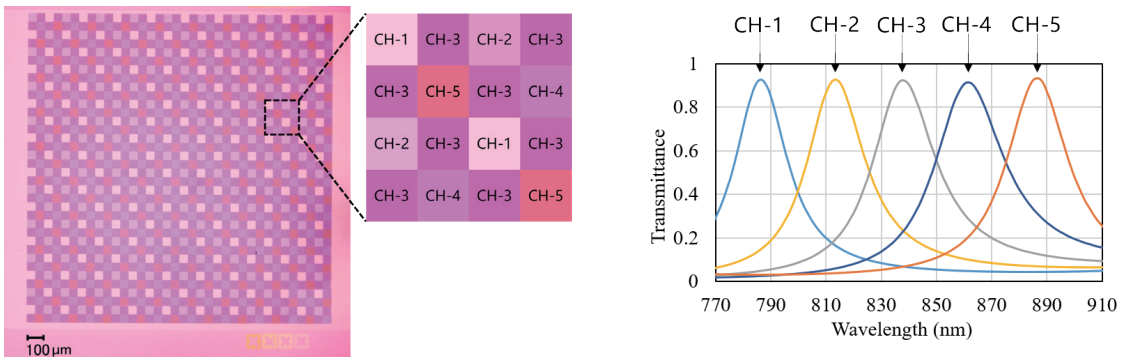

(a) (b)

Fig. 12. (Color online) (a) Photograph of a fabricated mosaic bandpass filter surface. The side length of a pixel of the image sensor was 7.5 μm and the side length of the mosaic pattern of the filter was 52.5 μm. (b) Measured spectral transmittance of each channel.

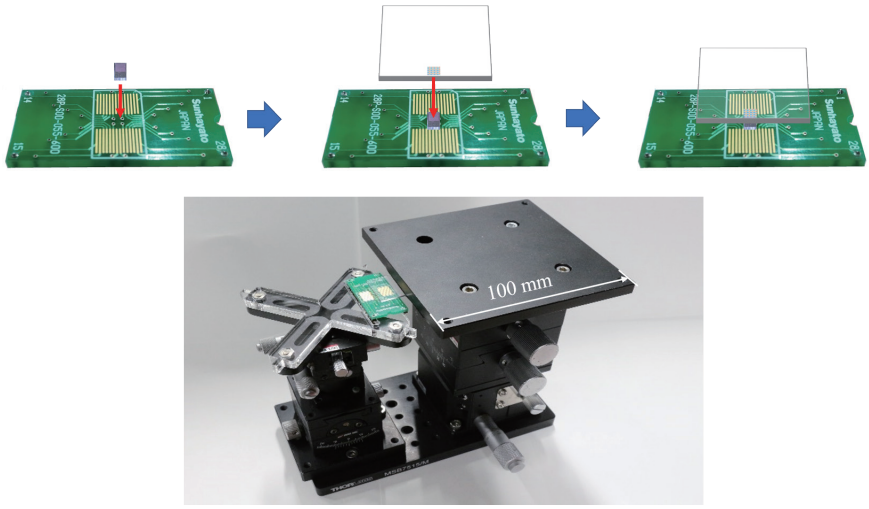

Fig. 13. (Color online) Appearance of the alignment device and schematic of filter adhesion.

measuring microscope. First, we set the filter glass on the right side of the alignment device and adjusted the platform's horizontal axis (α axis) to flatten the filter. Next, the circuit board was installed on the CMOS image sensor under the vision of a telecentric microscope. By adjusting the knobs on the left side ($XYZ\theta\alpha\beta$ axes) of the alignment device, we aligned the pixels of the CMOS image sensor with the filter channel. Then, the filter and the CMOS image sensor were glued together by UV light curing. The multichannel bandpass filter array will be used in the imaging system in our selfie fundus camera.

6. Conclusions

We designed a five-channel bandpass filter based on the principle of the interference filter that can operate in the NIR region for spectral detection in a selfie fundus camera. The bandpass filter was fabricated by sputtering, lithography, and etching. Before applying the fabricated filter to a fundus camera, we first set up a system to verify its performance by externally using it with different transmission wavelengths. The results showed that the filter can obtain a spectral intensity comparable to that of a spectrometer. Then, we verified that the filter could be used for quantitative detection by comparing the known input intensity and measurement data. Finally, we confirmed the effect of the number of channels on the performance of spectral reconstruction. The error was less than 15% of the maximum value within the measurement range of our proposed filter, even in the case of a five-channel filter. Future research opportunities based on the findings of this study include combining the bandpass filter array with a CMOS image sensor, obtaining pixel-based spectrum information, and achieving spectral detection in the NIR fundus camera.

Acknowledgments

This work was supported by Japan Science and Technology Agency, ACCEL (JPMJAC1601), VLSI Design and Education Center (VDEC), and The University of Tokyo in collaboration with Cadence Corporation and Mentor Graphics Corporation.

References

1 P. Hossain, J. Liversidge, M. J. Cree, A. Manivannan, P. Vieira, P. F. Sharp, G. C. Brown, and J. V. Forrester: Invest. Ophthalmol. Visual Sci. **39** (1998) 1879.
2 M. D. Abràmoff, M. K. Garvin, and M. Sonka: IEEE Rev. Biomed. Eng. **3** (2010) 169. https://doi.org/10.1109/RBME.2010.2084567
3 C. Cuspidi and C. Sala: J. Hypertens. **29** (2011) 33. http://doi.org/10.1097/HJH.0b013e328341c6b4
4 A. London, I. Benhar, and M. Schwartz: Nat. Rev. Neurol. **9** (2013) 44. https://doi.org/10.1038/nrneurol.2012.227
5 C. Y.-l. Cheung, Y. T. Ong, M. K. Ikram, S. Y. Ong, X. Li, S. Hilal, J.-A. S. Catindig, N. Venketasubramanian, P. Yap, D. Seow, C. P. Chen, and T. Y. Wong: Alzheimer's & Dementia. **10** (2014) 135. https://doi.org/10.1016/j.jalz.2013.06.009
6 M. K. Ikram, F. J. De Jong, E. J. Van Dijk, N. D. Prins, A. Hofman, M. M. B. Breteler, and P. T. V. M. De Jong: Brain **129** (2005) 182. https://doi.org/10.1093/brain/awh688
7 S. McGrory, J. R. Cameron, E. Pellegrini, C. Warren, F. N. Doubal, I. J. Deary, B. Dhillon, J. M. Wardlaw, E. Trucco, and T. J. MacGillivray: Alzheimer's & Dementia: Diagnosis, Assessment & Disease Monitoring. **6** (2017) 91. https://doi.org/10.1016/j.dadm.2016.11.001

8 D. Toslak, D. Thapa, Y. Chen, M. K. Erol, R. V. Paul Chan, and X. Yao: Opt. Lett. **41** (2016) 2688. https://doi.org/10.1364/OL.41.002688
9 K. Jin, H. Lu, Z. Su, C. Cheng, J. Ye, and D. Qian: BMC Ophthalmol. **17** (2017) 89. https://doi.org/10.1186/s12886-017-0484-5
10 H. Takehara, H. Sumi, W. Ze, T. Kondo, M. Haruta, K. Sasagawa, and J. Ohta: 2019 IEEE Biomedical Circuits and Systems Conf. (BioCAS, 2019) 1–4. https://doi.org/10.1109/BIOCAS.2019.8918695
11 H. Sumi, H. Takehara, S. Miyazaki, D. Shirahige, K. Sasagawa, T. Tokuda, Y. Watanabe, N. Kishi, J. Ohta, and M. Ishikawa: 2018 IEEE Symposium on VLSI Technology (VLSIT, 2018) 163–164. https://doi.org/10.1109/VLSIT.2018.8510698
12 Z. Wang, M. Uemura, H. Takehara, M. Haruta, H. Tashiro, K. Sasagawa, and J. Ohta: Jpn. J. Appl. Phys. **60** (2021) SBBL07. https://doi.org/10.35848/1347-4065/abea4c
13 G. Lu and B. Fei: J. Biomed. Opt. **19** (2014) 010901. https://doi.org/10.1117/1.JBO.19.1.010901
14 D. J. Mordant, I. Al-Abboud, G. Muyo, A. Gorman, A. Sallam, P. Ritchie, A. R. Harvey, and A. I. McNaught: Eye **25** (2011) 309. https://doi.org/10.1038/eye.2010.222
15 A. H. Kashani, E. Kirkman, G. Martin, and M. S. Humayun: PLoS One **6** (2011) e24482. https://doi.org/10.1371/journal.pone.0024482
16 A. Fawzi, N. Lee, A. Laine, J. Acton, and R. T. Smith: J. Biomed. Opt. **16** (2011) 106008. https://doi.org/10.1117/1.3640813
17 J. Schweizer, J. Hollmach, G. Steiner, L. Knels, R. H. W. Funk, and E. Koch: Biomed Tech. **57** (2012) 293. https://doi.org/10.1515/bmt-2012-4375
18 V. Nourrit, J. Denniss, M. M. K. Muqit, I. Schiessl, C. Fenerty, P. E. Stanga, and D. B. Henson: J. Français d'Ophtalmologie. **33** (2010) 686. https://doi.org/10.1016/j.jfo.2010.10.010
19 M. A. Sohrab, R. T. Smith, and A. A. Fawzi: Semin. Ophthalmol. **26** (2011) 156. https://doi.org/10.3109/08820538.2011.570848
20 R. E. Man, M. B. Sasongko, J. Xie, R. Kawasaki, W. J. Best, J. E. Noonan, C. D. Luu, J. J. Wang, and E. L. Lamoureux: Clinical & Experimental Ophthalmol. **43** (2015) 124. https://doi.org/10.1111/ceo.12387
21 B. Khoobehi, J. M. Beach, and H. Kawano: Invest. Ophthalmol. Visual Sci. **45** (2004) 1464. https://doi.org/10.1167/iovs.03-1069
22 L. Gao, R. T. Smith, and T. S. Tkaczyk: Biomed. Opt. Express **3** (2012) 48. https://doi.org/10.1364/BOE.3.000048
23 J. Kaluzny, H. Li, W. Liu, P. Nesper, J. Park, H. F. Zhang, and A. A. Fawzi: Curr. Eye Res. **42** (2017) 629. https://doi.org/10.1080/02713683.2016.1221976
24 H. Li, W. Liu, B. Dong, J. V. Kaluzny, A. A. Fawzi, and H. F. Zhang: J. Biophotonics **10** (2017) 830. https://doi.org/10.1002/jbio.201600053
25 H. A. Macleod: Thin-Film Optical Filters (CRC press, Boca Raton, 2017) 4th ed., Chap. 2.
26 T. D. Weber, J, Mertz: Biomed. Opt. Express., **9** (2018) 3867. https://doi.org/10.1364/BOE.9.003867
27 S. Martinez-Conde, J. Otero-Millan, and S. L. Macknik: Nat. Rev. Neurosci. **14** (2013) 83. https://doi.org/10.1038/nrn3405

About the Authors

Honghao Tang received her B.S. degree from Shaanxi Science and Technology University, China, in 2012 and her M.S. degree from Linkoping University, Sweden, in 2016. In 2020, she joined the Photonic Device Science Laboratory in the Graduate School of Material Science, Nara Institute of Science and Technology, Nara, Japan, as a Ph.D. candidate.
(tang.honghao.ti7@ms.naist.jp)

Hironari Takehara received his B.E. and M.E. degrees in applied chemistry from Kansai University, Osaka, Japan, in 1984 and 1986, respectively, and his Ph.D. degree in materials science from Nara Institute of Science and Technology (NAIST), Nara, Japan in 2015. From 1986 to 2012, he was a semiconductor process engineer at Panasonic Corporation, Kyoto, Japan, where he developed BiCMOS, high-voltage SOI, and optoelectronic IC processes. In 2015, he joined NAIST as a postdoctoral fellow and became an assistant professor in 2019. His current research interests involve CMOS image sensors and bioimaging. (t-hironari@ms.naist.jp)

Ze Wang received his B.E. and M.E. degrees in optical information science, and measuring and testing technologies and instruments from Xi'an University of Technology in 2015 and 2018, respectively. In 2019, he joined the Photonic Device Science Laboratory in the Graduate School of Material Science, Nara Institute of Science and Technology, Nara, Japan, as a Ph.D. candidate.

Noriaki Kishida received his B.E. degree from Kindai University in 2020. Currently, he is in the second year of his master's course at Nara Institute of Science and Technology, Japan. His research interests include fundus camera devices.

Makito Haruta received his B.E. degree in bioscience and biotechnology from Okayama University, Okayama, Japan, in 2009 and his M.S. degree in biological science and Dr. Eng. degree in material science from Nara Institute of Science and Technology (NAIST), Nara, Japan, in 2011 and 2014, respectively. He was a postdoctoral fellow with NAIST from 2014 to 2016. He joined the Institute for Research Initiatives, NAIST, in 2016, as an assistant professor. In 2019, he joined the Graduate School of Science and Technology, NAIST, as an assistant professor. His research interests include brain imaging devices for understanding brain functions related to animal behaviors. (m-haruta@ms.naist.jp)

Hiroyuki Tashiro received his B.E. and M.E. degrees in electrical and electronic engineering from Toyohashi University of Technology (TUT), Aichi, Japan, in 1994 and 1996, respectively. He received his Ph.D. degree in engineering from Nara Institute of Science and Technology (NAIST), Nara, Japan, in 2017. In 1998, he joined Nidek Co., Ltd., Aichi, Japan, where he worked on the research and development of ophthalmic surgical systems and retinal prostheses. In 2004, he joined the Faculty of Medical Sciences, Kyushu University, Fukuoka, Japan, as an assistant professor, and since 2019, he has also been an associate professor at NAIST. His current research interests include artificial vision systems and neural interfaces.
(tashiro.hiroyuki.289@m.kyushu-u.ac.jp)

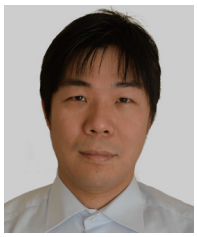

Kiyotaka Sasagawa received his B.S. degree from Kyoto University in 1999 and his M.E. and Ph.D. degrees in materials science from Nara Institute of Science and Technology (NAIST), Nara, Japan, in 2001 and 2004, respectively. He then became a researcher with National Institute of Information and Communications Technology, Tokyo. In 2008, he joined NAIST as an assistant professor, where he has been an associate professor since 2019. His research interests include bioimaging, biosensing, and electromagnetic field imaging (sasagawa@ms.naist.jp)

Jun Ohta received his B.E., M.E., and Dr. Eng. degrees in applied physics from The University of Tokyo, Japan, in 1981, 1983, and 1992, respectively. In 1983, he joined Mitsubishi Electric Corporation, Hyogo, Japan. From 1992 to 1993, he was a visiting scientist with the Optoelectronics Computing Systems Center, University of Colorado Boulder. In 1998, he joined the Graduate School of Materials Science, Nara Institute of Science and Technology (NAIST), Nara, Japan, as an associate professor. He was appointed as a professor in 2004. His current research interests include smart CMOS image sensors for biomedical applications and retinal prosthetic devices. He is a fellow of IEEE, the Japan Society of Applied Physics, and the Institute of Image, Information, and Television Engineers. (ohta@ms.naist.jp)